Kai Li
Zhichao Zhao
Songliang Chang
Jiawei Bao
Zhijiang Yuan
Xiaogang Jiang

http://dx.doi.org/10.21278/brod73404

ISSN 0007-215X
eISSN 1845-5859

RESEARCH ON DAMAGE CHARACTERISTICS AND PROTECTIVE STRUCTURE DESIGN OF STEEL PONTOONS UNDER NEAR-FIELD EXPLOSION LOAD

UDC 544.454:629.565.3
Original scientific paper

Summary

The focus of this paper is to investigate the damage characteristics and protective structure design of pontoons as an important barrier for the protection of ports. Two types of protective measures of pontoons are investigated: filling tanks with water and installing springs in tanks. In this paper, the damage characteristics of two types of pontoon side structures under the action of near-field explosion loads are simulated by using LS-DYNA explicit dynamic analysis software and the ALE algorithm. According to the numerical experiment results for filling different volumes of water in the side tanks, the volume of water for the minimum deformation of the shell plate is 100%, and for the first longitudinal bulkhead, it is 30-40%. Moreover, by applying weights to their deformations based on the actual explosion-proof performance requirements of the shell plate and the first longitudinal bulkhead, the pontoon side structure with the best explosion-proof performance can be obtained. The plastic deformation of the pontoon structure equipped with different types of springs is an order of magnitude smaller than that of the ordinary structure and of the pontoon structure filled with a water medium in the positive tanks. The explosive shock wave energy absorbed by the pontoon is effectively reduced by the addition of water or springs to the protective tanks. The minimum energy absorbed by the pontoon structure with water added in the protective tanks is 18.31% of the energy absorbed by the ordinary structure, and the corresponding volume ratio of water added in the protective tanks is 100%. The pontoon structure with springs in the side protection tanks absorbs only 7.2% of the energy absorbed by the ordinary structure. Both new side protection structures have demonstrated excellent explosion-proof performance.

Key words: *Near-field explosion; pontoon; ALE algorithm; structural design; water tank; spring*

1. Introduction

In today's world, the spread of terrorism seriously threatens the survival and development of all humans. It is of great significance to study the damage characteristics under the action of explosion loads and to improve the protective structure of pontoons, which can be used as protective barriers for coastal and offshore areas to prevent terrorist attacks from the sea.

At present, research on the explosion-proof performance of ships is much more prevalent than that of pontoons. Fragmentized warheads are mostly adopted by current anti-warship missiles [1], which usually invade the interior and explode at close range, resulting in combined shock wave and fragment damage to the structures [2]. Li et al. studied the deformation and damage of protective bulkheads in the form of a multi-layered composite structure, ship-stiffened plates, typical ship bulkhead structure, and hybrid corrugated sandwich plates under the synergistic effects of fragments and shock waves. The results indicate that the combined action of shock-wave load and high-speed fragments can enhance the shock damage effect differently from a simple superposition of the two load effects [2-5]. Zhao et al. studied the penetration effect of fragments with different shapes, masses, and slenderness ratios on the sides of the ship [6]. Kong et al. studied the defense effect of the ship's side protection tank on the explosion fragments and obtained a formula to calculate the residual velocity of the fragments [7]. In relation to the protection of the ship's side structure, Wang Yu et al. studied the dynamic response of warship sections with different shipboard protective structures subjected to an air contact explosion and discovered the relationship between intersection angles of wing plates and the protective performance of Y-shaped and V-shaped shipboard structures [8]. Yuan and Zhao studied the damage mechanism of a ship's protective structure under an underwater contact explosion load [9]. Zhang and Gao studied a ship's local structure damage effect when subjected to an underwater explosion [10]. Guan et al. studied the dynamic response of the cargo hold structure of the first CNG (Compressed Natural Gas) carrier in the world under a gas explosion load [11]. Zhang et al. studied the time course of the deflection of a thin plate made of 921A steel in different initial conditions under an impact load [12]. Chen et al. studied the influence of flat steel on an explosive load inside a closed tank [13]. Liu et al. used the FSI (Fluid-Structure-Interaction) model to conduct a numerical study on the global responses of a surface ship subjected to an underwater explosion in waves and validated the numerical model by carrying out an underwater explosion experiment [14]. Based on the SPH (Smoothed Particle Hydrodynamics) method, Ming et al. studied flat plates subjected to underwater contact explosions with the application of a combined damage variable [15]. Veić et al. investigated the effect of breaking wave shape on impact load on a monopile structure by numerical simulation [16].

As for research on pontoons, Jiang et al. simulated the shock response of a floating platform subjected to a far-field explosion load using a method to load the shock directly on the surface exposed to explosion in the calculation region [17]. Yang et al. studied the hydrodynamic performance of water-ballast type pontoons, pile-supported OWC (Oscillating Water Column) breakwater and anti-rolling type pontoons, F-type pontoons, and T-shaped pontoons [18-22]. Dai presents a literature review on the research and development of pontoons [23].

In summary, the hydrodynamic performance of pontoons is the focus of existing research, but there are few research studies on the explosion-proof performance of pontoons. Such pontoons can only facilitate the management of areas such as ports, offshore farms, and beaches, but they cannot prevent terrorist attacks and pirate attacks that may come from the sea. To use pontoons more effectively for anti-terrorism, this paper focuses on the damage

characteristics of pontoons under near-field explosion loads and designs pontoons with several new side structures to enhance their explosion-proof performance.

2. Fluid-solid coupling algorithm

The simulation calculation in this paper relies on the explicit dynamic analysis software LS-DYNA. LS-DYNA provides three coupling algorithms, Lagrange, Euler and ALE, for users to choose from. The Lagrangian method is commonly used in solid mechanics for stress-strain analysis [24]. Based on the material coordinates, the mesh described by this algorithm is integrated with the computational structure, that is, its finite element nodes are the material points, so the deformation of its structure is exactly the same as that of the finite element model. The advantage of this algorithm is that it can describe the motion of the boundary of the structure very accurately, but it is not helpful for dealing with the large deformation of the structure. The Eulerian method is mostly used for the analysis of fluid mechanics. Based on spatial coordinates, the mesh and material analyzed by the Eulerian method are independent of each other. The node of the finite element is the space point, whose position is always the original spatial position, that is, its mesh size and position are always constant. The advantage of the Eulerian method is that it allows material to flow between meshes. ALE method is first applied to the finite difference method of the numerical simulation of fluid dynamics, which has advantages of both the Lagrangian method and the Eulerian method and can simultaneously deal with the large spatial displacement and deformation of the structure. Wang et al. performed numerical investigations on three dimensional hydroelasticity characteristics of imperfect lattice sandwich panel subjected to water entry based on ALE method [25]. In this paper, ALE method is used to simulate near-field explosions near the water surface.

When using ALE method, a third reference coordinate system other than the Lagrangian and Eulerian coordinate systems is introduced, and the material derivative of the reference coordinate can be expressed as:

$$\frac{\partial f(X_i,t)}{\partial t}=\frac{\partial f(x_i,t)}{\partial t}+w_i\frac{\partial f(x_i,t)}{\partial t} \tag{1}$$

where X_i is the Lagrangian coordinate, x_i is the Eulerian coordinate, w_i is the relative velocity, and $f()$ is the general form of field functions such as mass, velocity, pressure and so on.

The relative velocity $\boldsymbol{w}$ is introduced to make $\boldsymbol{w}=\boldsymbol{v}-\boldsymbol{u}$, where $\boldsymbol{v}$ represents the velocity of the material and $\boldsymbol{u}$ represents the velocity of the finite element mesh. The control equation of the ALE algorithm is:

(1) Mass conservation equation

$$\frac{\partial \rho}{\partial t}=-\rho\frac{\partial v_i}{\partial x_i}-w_i\frac{\rho}{\partial x_i} \tag{2}$$

where ρ is the fluid density.

(2) Momentum conservation equation

$$v\frac{\partial v_i}{\partial t} = \frac{\partial \sigma_{ij}}{\partial x_j} + \rho b_i - \rho w_j \frac{\partial v_i}{\partial x_j} \tag{3}$$

where b_i is the body force of micro unit and σ_{ij} is the stress tensor, which can be expressed as:

$$\sigma_{ij} = -p\delta_{ij} + \mu(v_{i,j} + v_{j,i}) \tag{4}$$

where p is the pressure, μ is the dynamic viscosity, δ_{ij} is the Kronecker function, and $v_{i,j} = \frac{\partial v_i}{\partial x_j}$, $v_{j,i} = \frac{\partial v_j}{\partial x_i}$.

Equation (4) can be solved simultaneously with the following boundary conditions and initial conditions:

$$v_i = U_i^0 \text{ on domain } \Gamma_1 \tag{5}$$

$$\sigma_{ij} n_j = 0 \text{ on domain } \Gamma_2 \tag{6}$$

In equations (5) and (6):

$$\Gamma_1 \cup \Gamma_2 = \Gamma \tag{7}$$

$$\Gamma_1 \cap \Gamma_2 = 0 \tag{8}$$

In the above formula, Γ denotes the complete boundary of the computational domain, and Γ_1 and Γ_2 are parts of Γ. The superscript is the initial specified value of the parameter, n_j is the unit vector of the normal line outside the boundary, and δ_{ij} is the Kronecker function. Assuming that the velocity field of the computational domain is known at time t = 0, it is:

$$v_i(x_i, 0) = 0 \tag{9}$$

(3) Energy conservation equation

$$\rho\frac{\partial E}{\partial t} = \sigma_{ij} v_{i,j} + \rho b_i - \rho w_j \frac{\partial E}{\partial x_j} \tag{10}$$

where ρ represents the material density, σ_{ij} is the Cauchy's stress tensor, E is the internal energy per unit mass, and b_i is the body force of the micro unit.

3. Numerical simulation of the damage to a pontoon under a near-field explosion load

To ensure that the pontoon can effectively protect relevant facilities in the event of terrorist attacks, it is necessary to conduct a targeted study on the damage characteristics of the pontoon in the case of an explosion and take measures to improve its explosion-proof performance. In this paper, several new types of side protection structures are designed based on the calculations for ordinary structure and the study of their damage characteristics.

3.1 Configuration of pontoon structure

The pontoon analyzed in this paper is a steel floating structure with a length of 30m, a width of 8m, and a height of 4m that is divided into 24 tanks by three transverse bulkheads, four longitudinal bulkheads, and one center longitudinal bulkhead. Each tank is numbered for ease of description, as shown in Figure 1.

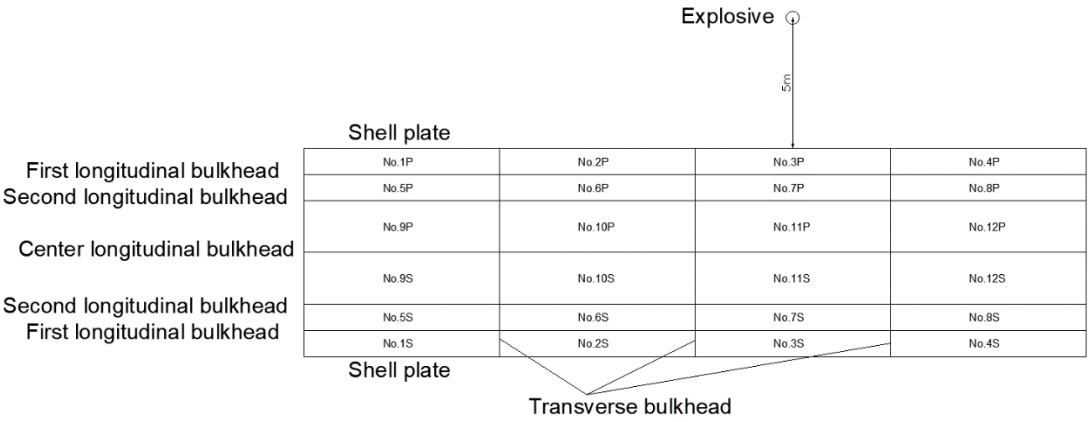

Figure 1. Distribution of the left-side tanks in the pontoon and the location of the explosive

The longitudinal stiffeners are installed on the shell plate, longitudinal bulkhead, deck, and bottom plate of the pontoon. Vertical stiffeners are installed on the transverse bulkhead, and horizontal girders with T-shaped sections are installed in the middle of the bulkhead. The transverse bulkhead structure is shown in Figure 2. The pontoon's frame spacing is 0.5m, and the frame is a T-shaped section. The typical transverse section is shown in Figure 3.

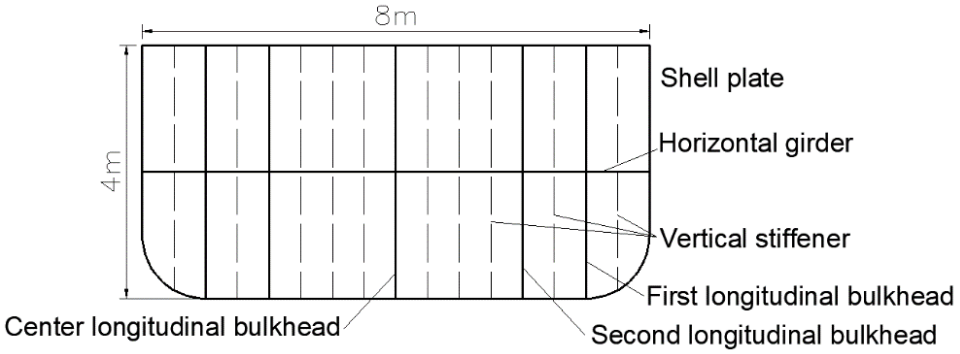

Figure 2. Typical transverse bulkhead

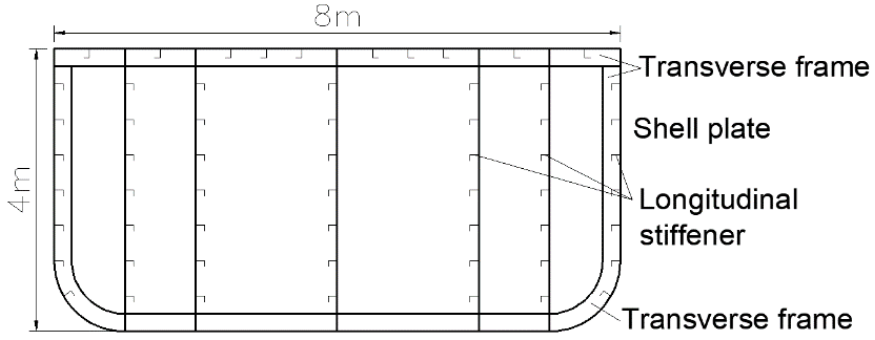

Figure 3. Typical transverse section

In the follow-up, the explosion-proof performance of the ordinary structure model described above and the new pontoon structure improved on the basis of the ordinary structure will be compared and analyzed.

3.2 The assumed explosion scenario and material model

A near-field explosion is a common explosion condition of pontoons because the wave-eliminating devices placed on the periphery of the pontoon have an isolation effect on the proximity of the explosives. In this paper, the location of the explosive is 5m away from the center of Tank No. 3, and the lowest point of the explosive is 200mm above the water surface, as shown in Figure 1. The mass of the explosive is 300kg, which can produce a total of 1.69×10^6 kJ detonation energy.

Figure 4 shows the typical explosion scenario for the pontoon. Generally, the pontoon should be fixed at the working place by using several mooring lines. However, the mooring system was not included in the FE modeling to reduce CPU (Central Processing Unit) consumption for numerical analysis. Figure 5 (a) shows the transverse section of the pontoon structure with the surrounding air and water. In the entire computational domain, the dimensions of the air domain are 32000mm × 24000mm × 4,500mm, and the dimensions of the water domain are 32,000mm × 24000mm × 5,500mm. The entire computation model is shown in Figure 5 (b).

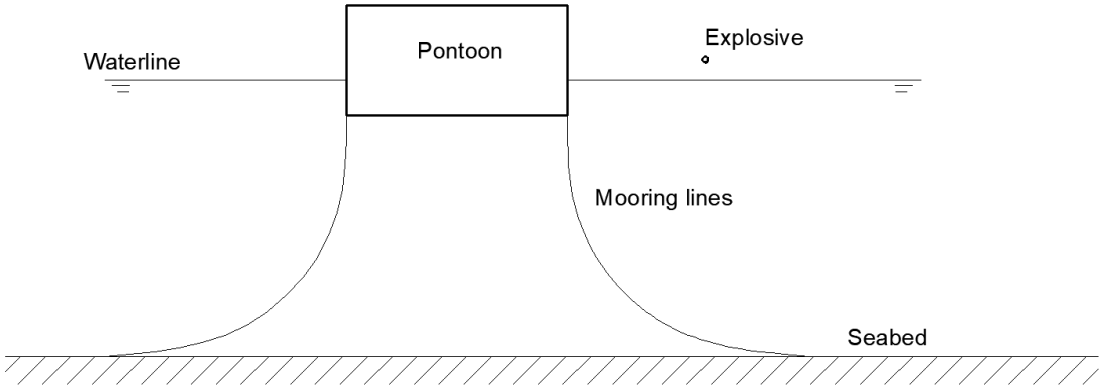

Figure 4. The assumed explosion scenario

As for the fluid medium, *MAT140_VACUUM is selected as the material type of the air and *MAT009_NULL is selected as the material type of the water. The state equation of GRUNEISEN is used to describe water, as is shown in Formula (11):

$$p = \frac{\rho_0 C^2 \mu \left[1+\left(1-\frac{\gamma_0}{2}\right)\mu - \frac{a}{2}\mu^2\right]}{\left[1-(S_1-1)\mu - s_2\frac{\mu^2}{\mu+1} - s_3\frac{\mu^3}{(\mu+1)^2}\right]} + (\gamma_0+\alpha\mu)E \tag{11}$$

In Formula (11), C is the propagation speed of sound in water; α is the first-order correction to the GRUNEISEN coefficient, γ_0; S_1、S_2、S_3 is the dimensionless coefficient of the slope of the $u_s - u_p$ curve, u_s is the velocity of the shock wave, u_p is the velocity of the fluid particle, E is the volume internal energy of the water, and μ is the volume change rate of the water.

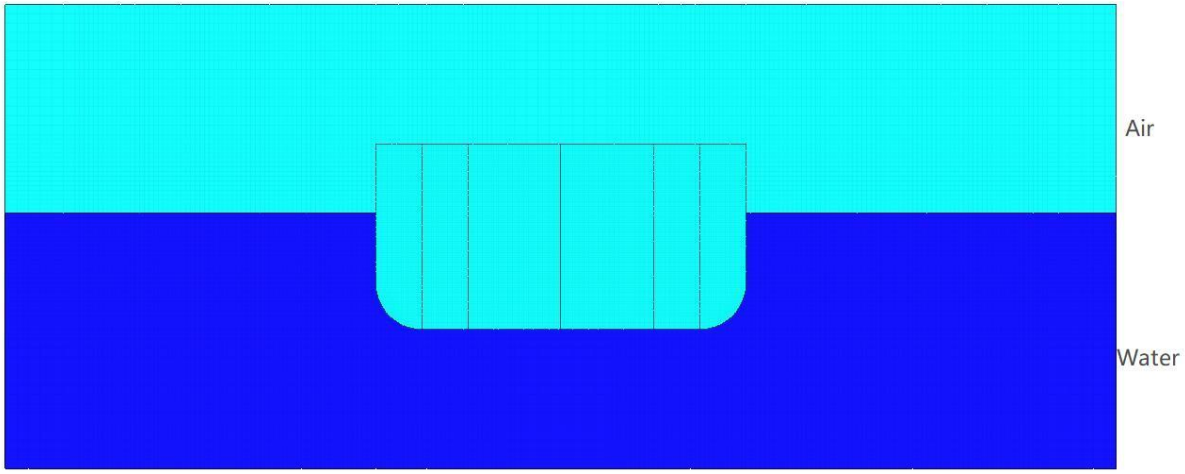

(a) Transverse section of the pontoon structure

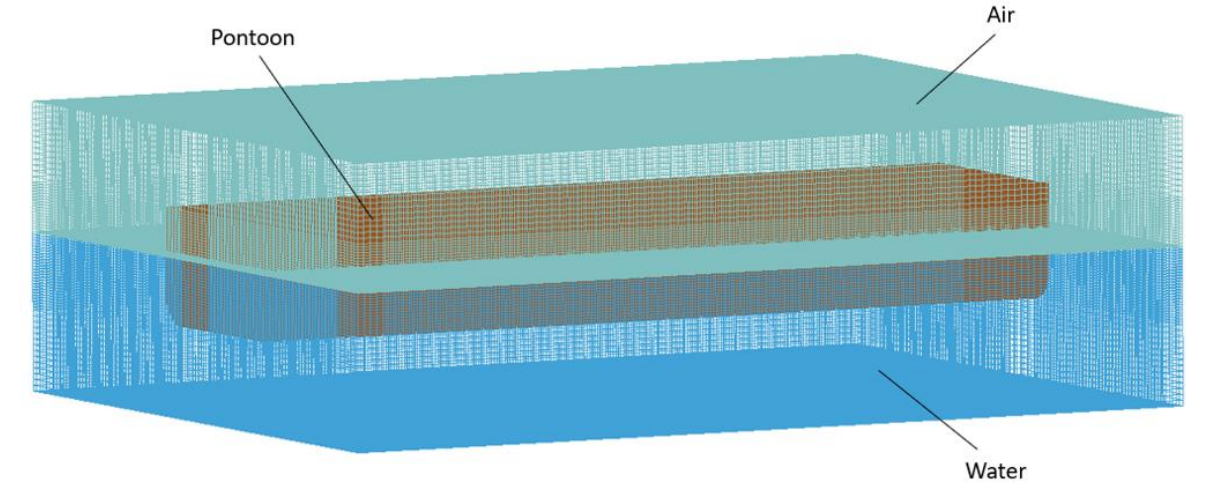

(b) Entire computational domain

Figure 5. Computational model

Table 1 shows the parameters of the equation of the state for water, where E_0 is the initial volume internal energy of the water and V_0 is the initial relative volume of the water.

Table 1. Parameters of the equation of state for water

Main parameter	Value
C (m/s)	1,480
α	1.92
S_1	-0.096
S_2	0
S_3	0.5
E_0	0
V_0	0

Low alloy steel Q345 is adopted as the structural material of the pontoon structure, the JOHNSON_COOK model is adopted as the constitutive model for shell elements [15], and the PLASTIC_KINEMATIC model is adopted for the beam elements. The explosive chosen is composition C-4, the material model of explosives adopts the HIGH_EXPLOSIVE_BURN model, and the equation of the state for C-4 explosives uses the JWL equation [17]. The FE model of the port side of the pontoon is shown in Figure 6.

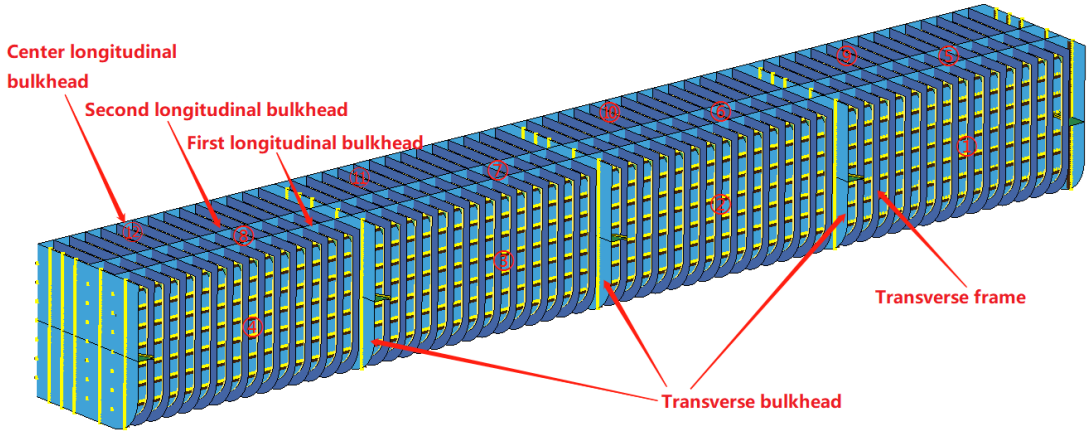

Figure 6. The finite element model for the port side (deck and shell plate are hidden)

For this model, fully fixed constraint is applied to the nodes in the four corner areas at both ends of the pontoon, that is, Ux=0; Uy = 0; Uz = 0; Rx = 0; Ry = 0; and Rz = 0. The boudary conditions of the pontoon structure are shown in Figure 7. The boundary conditions of the computational domain were modeled by setting the translational velocities of the nodes on all sides of the region of fluid to zero. An outflow boundary condition was also used on all sides of the region of the fluid modeled. The outflow boundary condition allowed the blast waves to exit the region of air and water without reflecting back to the pontoon.

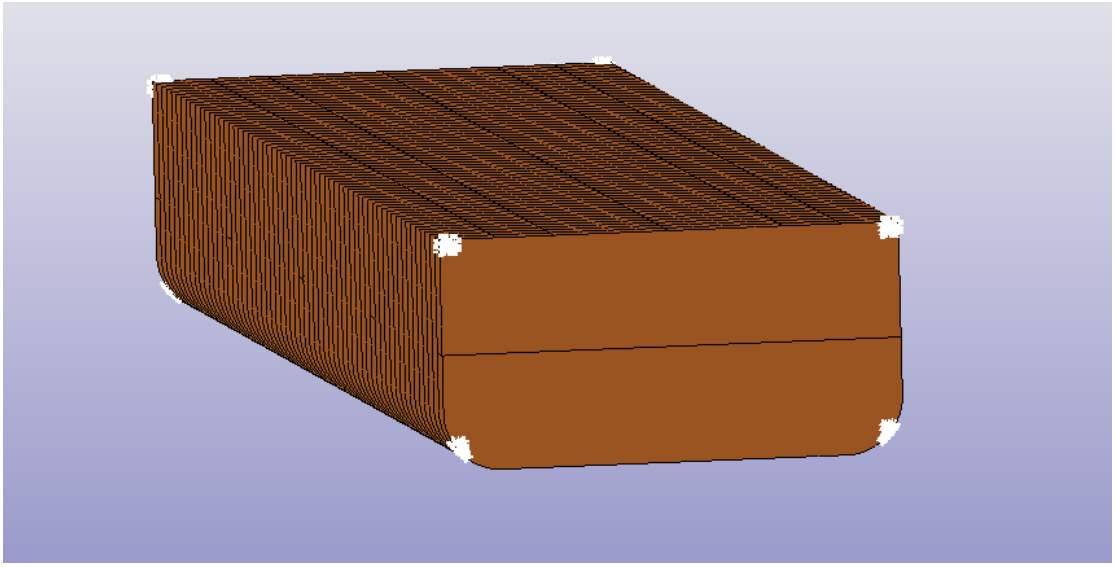

Figure 7. Boundary conditions of the pontoon structure

3.3 Numerical model calibration

To provide a basis for the estimation of peak overpressure of an air blast wave, many researchers have derived various expressions based on empirical or semi-empirical approaches, and these expressions for overpressure calculation mainly depend on scaled distance (Z), which is the ratio of stand-off distance (R) and the cubic root of the charge weight (W). For example, the expression derived by Naumyenko and Petrovshyi [26] is:

$$p_{so} = \begin{cases} -0.1 + \frac{1.07}{Z^3}, Z \leq 1\mathrm{m/kg}^{1/3} \\ \frac{0.076}{Z} + \frac{0.255}{Z^2} + \frac{0.65}{Z^3}, 1\mathrm{m/kg}^{1/3} < Z \leq 15\mathrm{m/kg}^{1/3} \end{cases} \quad (12)$$

Z is the scaled distance and can be expressed as:

$$Z = \frac{R}{\sqrt[3]{W}} \quad (13)$$

where R is the stand-off distance and W is the explosive charge weight.

Following Equation (12), in the assumed explosion scenario, the peak overpressure of a 300kg explosive with a 9m stand-off distance would be 0.4655MPa.

To verify the mesh sensitivity, different mesh sizes were created, and the peak overpressure of the blast was monitored and compared. Three mesh sizes of 50mm, 100mm, and 200mm were used to determine the mesh sensitivity of the numerical simulation to mesh size and determine the best mesh size to balance accuracy and computational cost. The mesh sensitivity analysis was run in the assumed explosion scenario. Figure 8 shows the simulated overpressure curves of the pontoon under near-field explosion loads by using three mesh sizes. Table 2 presents a summary of the peak overpressures obtained by simulation and the peak overpressure estimated by using Equation (12).

Table 2. The estimated and numerically obtained peak overpressures

Mesh size(mm)	Peak overpressure(MPa)	Ratio of the numerically obtained value to the estimated value	p_{so} (MPa)
50	0.457	0.9817	0.4655
100	0.4545	0.9764	
200	0.4428	0.9512	

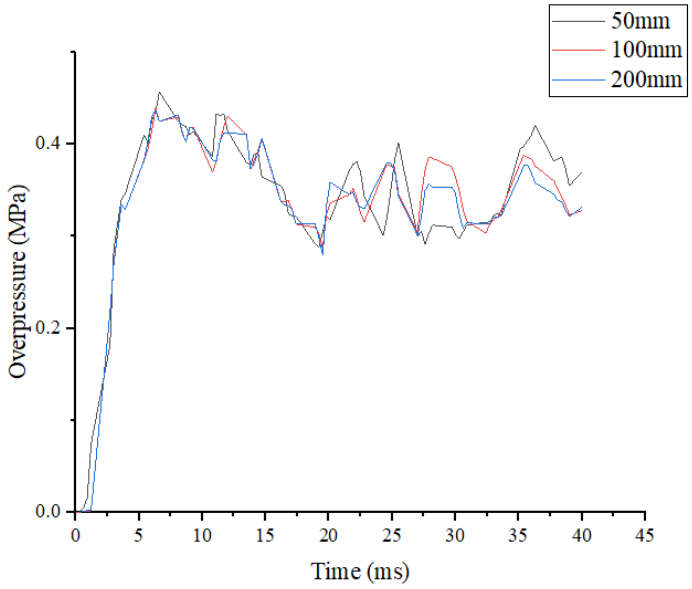

Figure 8. Maximum pressure diagram of pontoon structure under explosion load under three grids

It can be seen from Table 2 that all three numerically obtained peak overpressures corresponding to three mesh sizes are very close to the estimated peak overpressure. At the same time, the results of the three curves are very similar, and the trend is basically the same. Although the 50mm mesh size gave a higher degree of deflection accuracy, the computational cost was too high. A mesh size of 100 mm was used for the numerical simulation because it gave a reasonable degree of accuracy in terms of peak overpressure without significantly increasing the computational cost.

3.4 Calculation results of ordinary structure

It is necessary to select different elements and nodes at different positions on the pontoon as observation points for analysis and research to facilitate a comprehensive analysis of the damage to the pontoon structure. As shown in Figures 9 and 10, a series of shell elements on the shell plate and the first longitudinal bulkhead of Tank No. 3 are taken as observation points because the explosive is facing Tank No. 3.

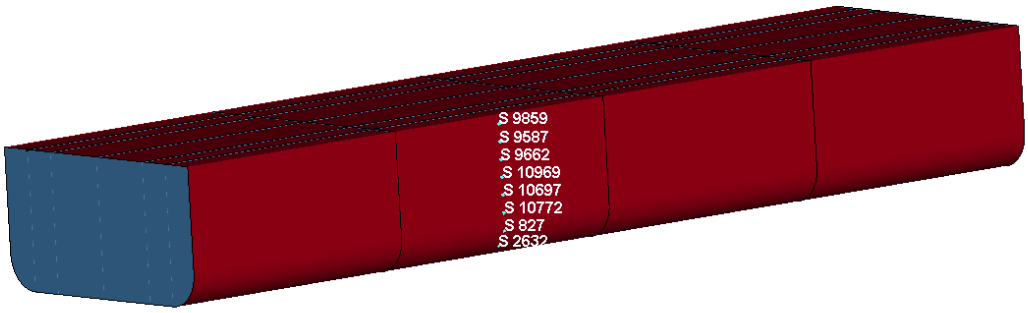

Figure 9. Distribution of observation points on the shell plate

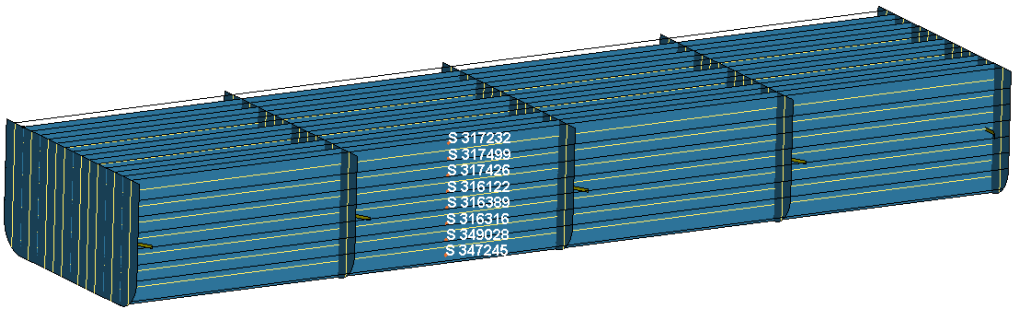

Figure 10. Distribution of observation points on the first longitudinal bulkhead

The deformation duration curves of the normal direction of the aforementioned observation point are extracted, as shown in Figures 11 and 12.

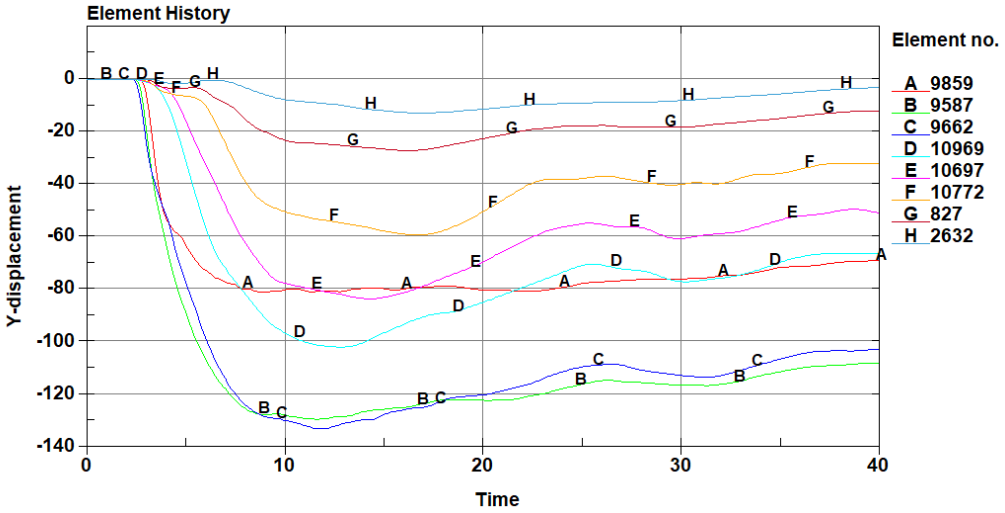

Figure 11. Deformation duration curves of shell plate observation points

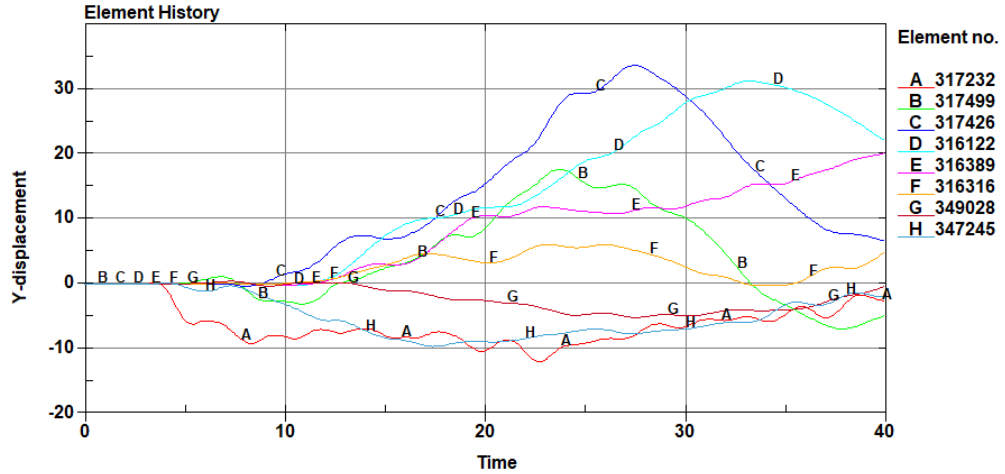

Figure 12. Deformation duration curves of first longitudinal bulkhead observation points

The deformation results of the pontoon structure after explosion are shown in Figure 13.

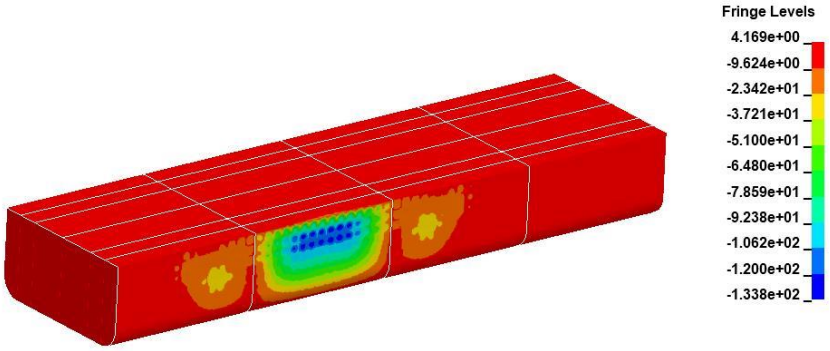

(a) Deformation results of the pontoon structure at 10ms

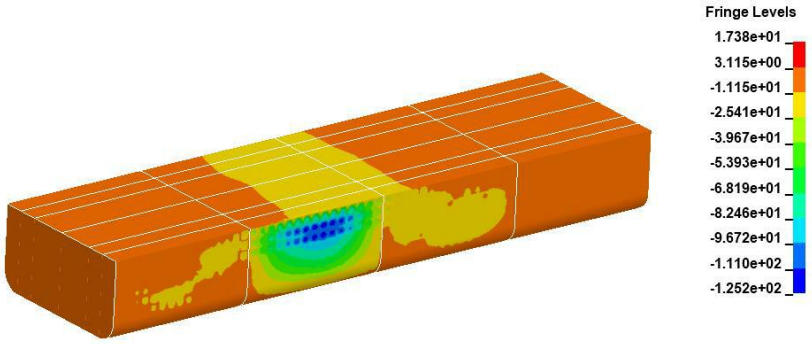

(b) Deformation results of the pontoon structure at 20ms

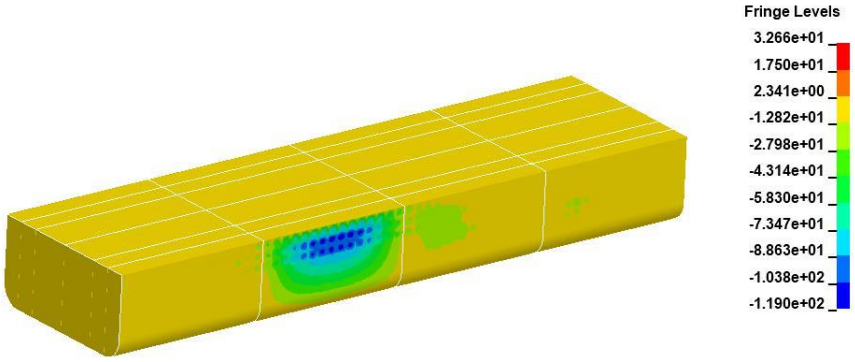

(c) Deformation results of the pontoon structure at 30ms

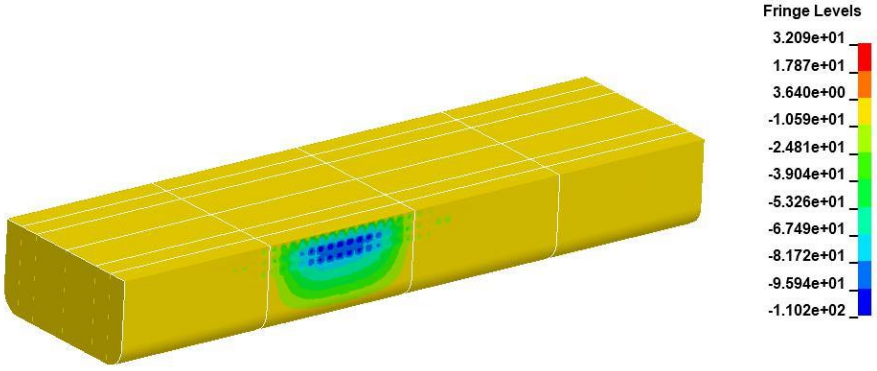

(d) Deformation results of the pontoon structure at 40ms

Figure 13. Deformation results of the pontoon structure after explosion

The maximum deformation and maximum plastic deformation of the shell plate are 135.9mm and 110.3mm, respectively, while the corresponding data for the first longitudinal bulkhead is 33.2mm and 22.6mm, obtained by analyzing their deformation curves. The maximum deformations of the shell plate and the first longitudinal bulkhead occur at 12.1ms and 27.8ms after the explosion, respectively, which is due to the asynchronism of the deformation caused by the difference of 1m between the two longitudinal bulkheads and the explosive. The extracted stress response curves of the observation points are shown in Figures 14 and 15.

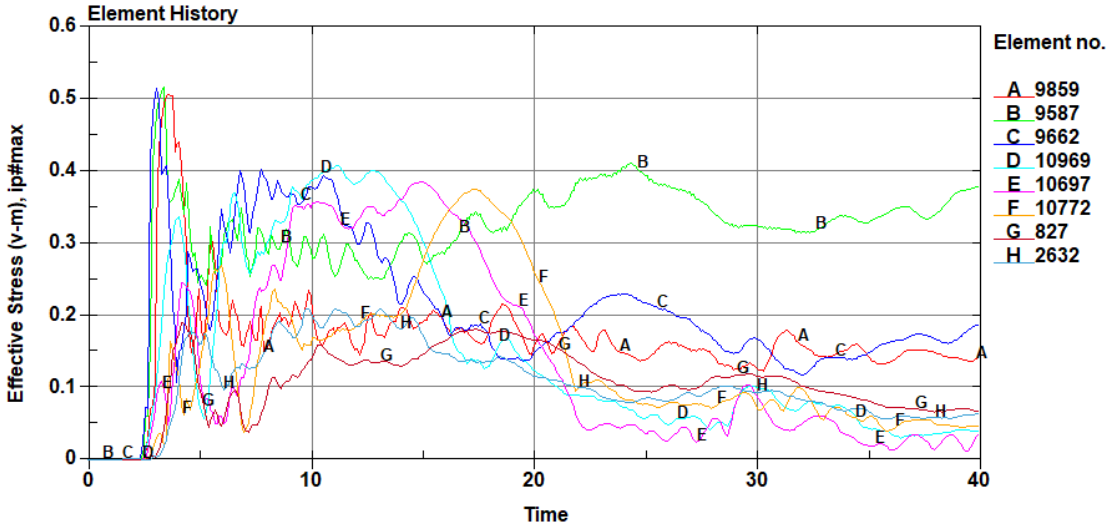

Figure 14. Stress response curves of shell plate observation points

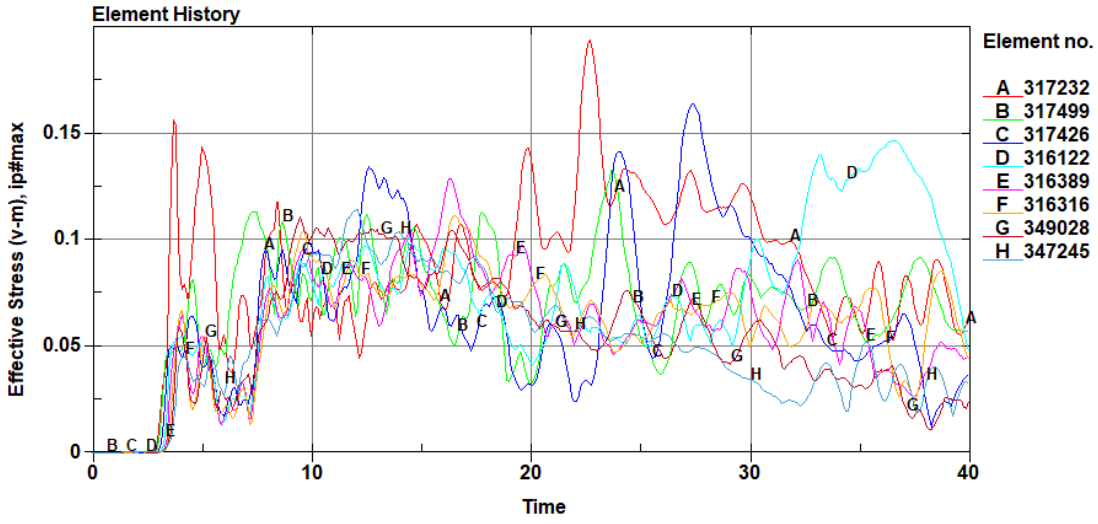

Figure 15. Stress response curves of first longitudinal bulkhead observation points

The stress results of the pontoon structure after explosion are shown in Figure 16.

An analysis of the above stress response curve shows that the maximum stress value of the shell plate is the stress value of element A at 4.1ms, which is 593.3MPa. Although the maximum stress value of the shell plate exceeds the yield strength of Q345 steel, it does not exceed the ultimate strength of Q345 steel, which means that although the shell plate produces plastic deformation, it does not break. The maximum stress of the first longitudinal bulkhead is 190MPa, which is lower than the yield strength, and its explosion-proof performance and water tightness are maintained.

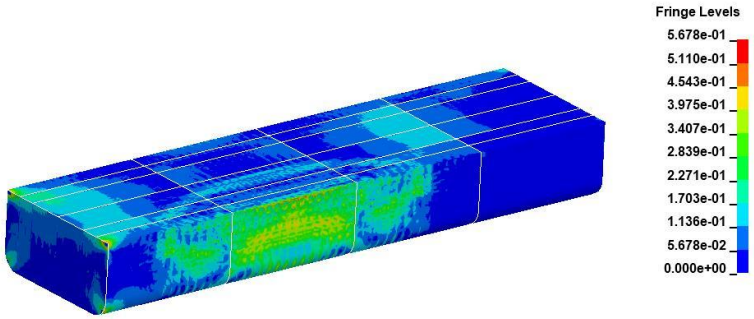

(a) Stress results of the pontoon structure at 10ms

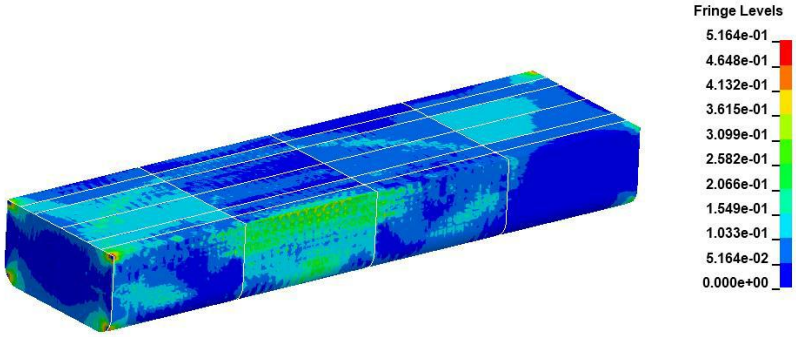

(b) Stress results of the pontoon structure at 20ms

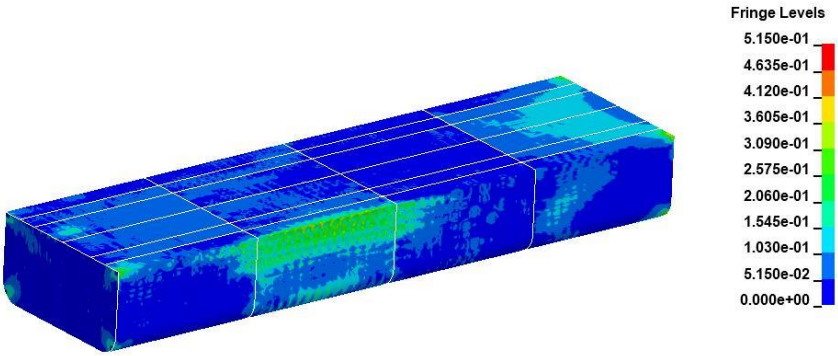

(c) Stress results of the pontoon structure at 30ms

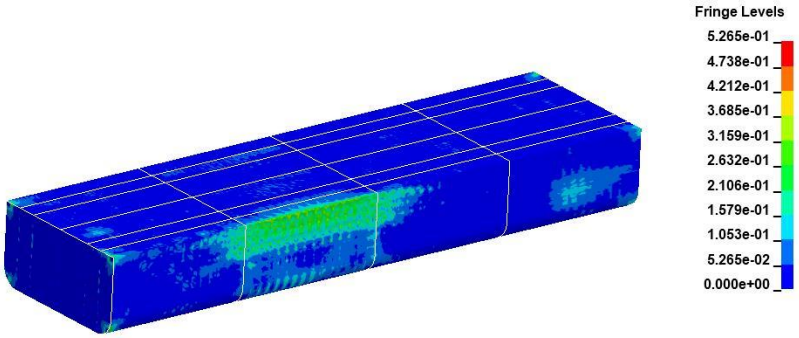

(d) Stress results of the pontoon structure at 40ms

Figure 16. Stress results of the pontoon structure after explosion

4. Structural design of protective tanks

To improve the explosion-proof performance of the pontoon, two new types of pontoon side structures are proposed in this chapter, and their explosion-proof performances are analyzed and compared with ordinary structure. The new types of protective structures refer to Tanks No. 1, 2, 3, and 4 in the pontoon as protective tanks, into which either water mediums or springs are added, and the damage characteristics of the three different structures are compared in the same explosive impact environment.

4.1 Structural model of protective tanks

4.1.1 Filling water medium in the protective tanks

The water that accounts for 10%, 20%, 30%, 40%, 50%, 60%, 70%, 80%, 90%, and 100% of the total volume of the tanks is filled in Tanks No. 1, 2, 3, and 4 of the pontoon. The corresponding finite element model is shown in Figure 17.

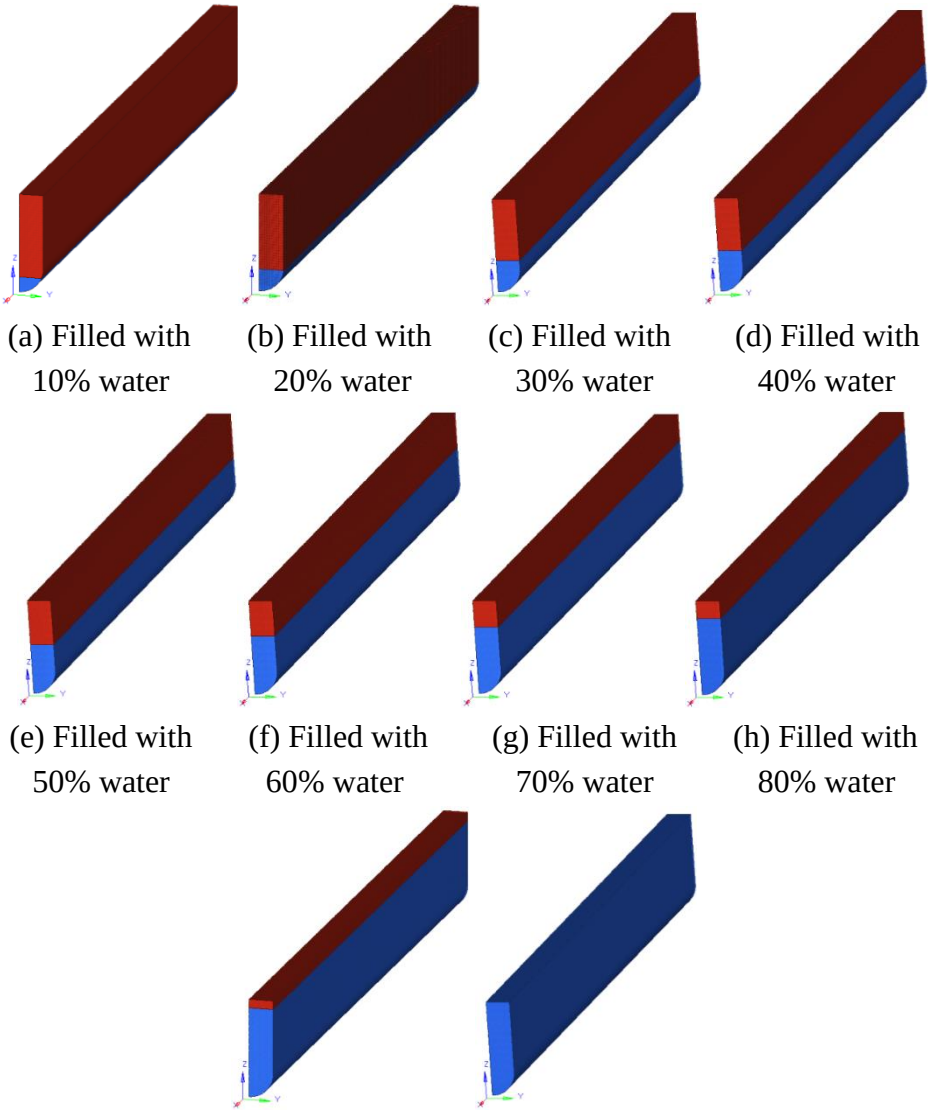

(a) Filled with 10% water (b) Filled with 20% water (c) Filled with 30% water (d) Filled with 40% water

(e) Filled with 50% water (f) Filled with 60% water (g) Filled with 70% water (h) Filled with 80% water

(i) Filled with 90% water (j) Filled with 100% water

Figure 17. Water filling model with different volume ratios

4.1.2 Assemble springs in protective tanks

Different types of springs connected to the shell plate and the first longitudinal bulkhead are assembled in Tanks No. 1, 2, 3, and 4 in the pontoon. A total of five different types of springs are designed, and the spring data is shown in Table 3.

Table 3. Spring parameters

Spring	Diameter(mm)	Pitch diameter(mm)	Total coils	Spring stiffness(KN/mm)
Model 1	70	200	11	3.27
Model 2	80	200	11	5.58
Model 3	80	300	9	2.13
Model 4	100	230	10	10.08
Model 5	100	300	8	6.057

The explosion environment parameters for all structures are the same as that described in 3.2, and the selection of observation points is the same as that shown in Figures 9 and 10, so as to facilitate the comparison of the explosion-proof performance of each structure.

4.2 Damage characteristics of new protective structure

In this chapter, the structural response of the new protective structure proposed in Section 4.1 under the near-field explosion load will be studied. The plastic deformation and energy data of each observation point are extracted as research objects and normalized to dimensionless numbers to facilitate data analysis. The dimensionless parameters are defined as follows:

$$\varepsilon = \frac{\varepsilon_1}{b} \times 100 \tag{14}$$

where ε is the relative value of plastic deformation, ε_1 is the plastic deformation value, and b is the width of the pontoon.

$$E = \frac{E_1}{E_0} \times 1000 \tag{15}$$

where E is the relative value of pontoon energy, E_1 is the energy value of the pontoon structure, and E_0 is the energy produced by the explosion of 300kg composition C-4, 1.69×10^9J.

The damage characteristics of each protective structure under the near-field explosion load will be analyzed below according to the dimensionless parameters defined above.

Plastic deformation is an important parameter for studying the damage characteristics of the pontoon structure after being subjected to explosive loading. After normalizing the plastic deformation data of the structure, the curves shown below can be used to analyze the explosion-proof performance of the two new structures.

(1) Plastic deformation of pontoon structure filled with water medium in protective tanks

The dimensionless results of plastic deformation of the shell plate and the first longitudinal bulkhead of the pontoon filled with a water medium in the protective tanks are shown in Figures 18 and 19.

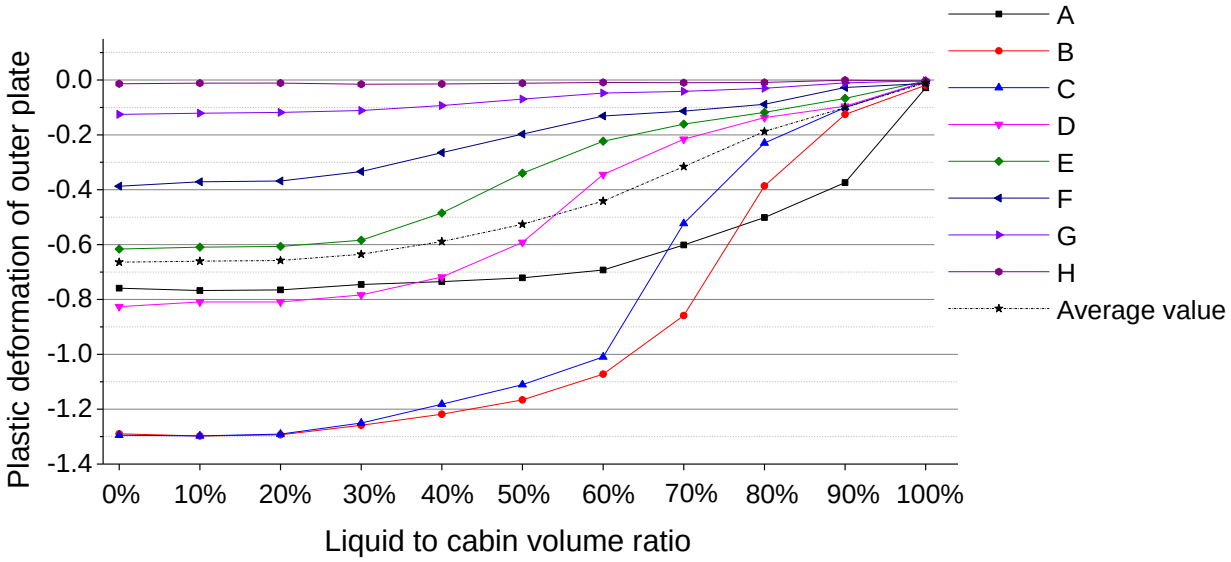

Figure 18. Plastic deformation of the shell plate after filling the water medium in the protective tanks

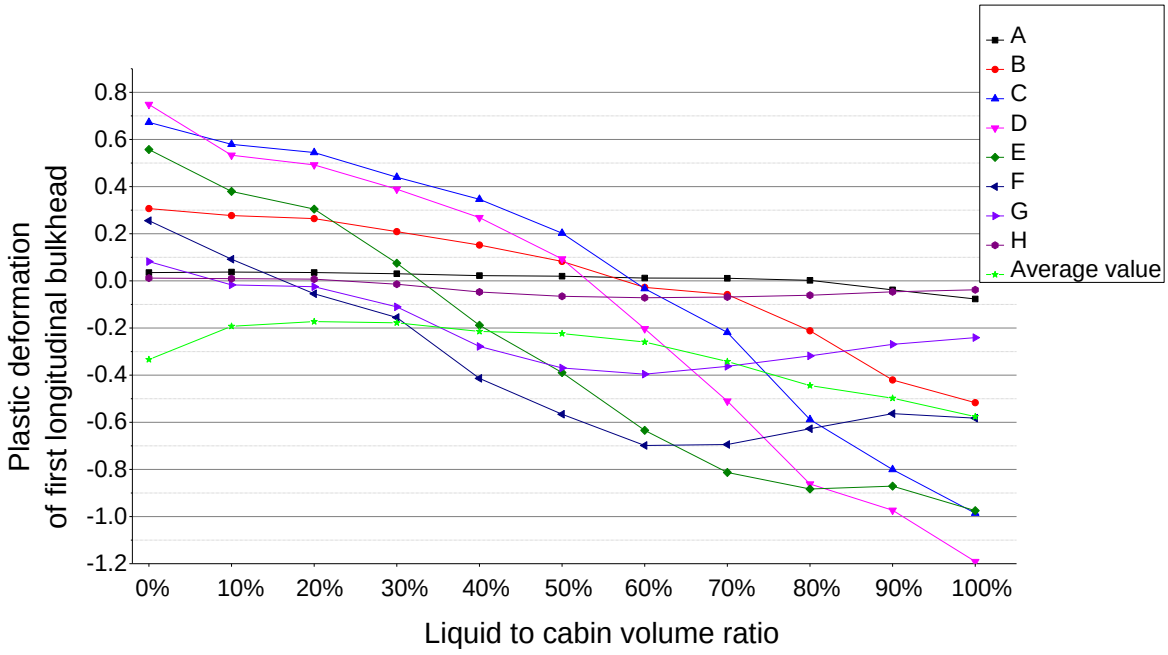

Figure 19. Plastic deformation of the first longitudinal bulkhead after filling the water medium in the protective tanks

A, B, C, D, E, F, G, and H in Figures18 and 19 represent the plastic deformation values of each observation point. The average value in Figure 18 refers to the average value of plastic deformation at the observation points of each protective structure, while the average value in Figure 19 refers to the average value of the negative absolute value of plastic deformation at the observation points of each protective structure. It can be seen from the observation of Figure 18 that the plastic deformation of the shell plate decreases as the volume of water injected into the protective tanks increases. From the curve of the average value, when the water injection volume reaches 60% of the volume of the tanks, the plastic deformation of the shell plate is reduced to 66.4% of that of the ordinary structure. From that point, the plastic deformation of the shell plate begins to decrease significantly as the injection

volume of the water increases. When the protective compartment is filled with water, the plastic deformation of the shell plate is only 1.5% of the ordinary structure, which demonstrates its superior protection performance.

It can be seen from Figure 18 that the plastic deformation of the first longitudinal bulkhead changes from positive to negative with the increase in the volume of water injected into the tanks—that is, the deformation direction of the first longitudinal bulkhead changes (the positive direction of the deformation is perpendicular to the first longitudinal bulkhead toward the shell plate and the explosive). This is because as the amount of water injected increases, the pressure generated by the deformation of the shell plate transferred to the first longitudinal bulkhead through water increases, which changes the deformation direction of the first longitudinal bulkhead. The more water that is injected, the more obvious the change is. When the tank is full of liquid, the plastic deformation of the shell plate is minimal, but the plastic deformation of the first longitudinal bulkhead reaches a maximum. This is because there is no space above the liquid for it to flow to, and more of the pressure transferred from the shell plate to the liquid will be transferred to the surrounding area. On the one hand, this enhances the ability of the liquid as a buffer substance to alleviate the deformation of the shell plate. On the other hand, it transfers more pressure to the first longitudinal bulkhead and enlarges its deformation, which results in the deformation of the first longitudinal bulkhead being larger than that of the ordinary structure. It can be seen from the average curve that the volume of water injection that minimizes the plastic deformation of the first longitudinal bulkhead is 30-50%, and the plastic deformation is correspondingly reduced to 53-66% of the ordinary structure, which reflects its good protective performance.

Because the water injection volume that minimizes the plastic deformation of the shell plate is not the same as for the first longitudinal bulkhead, it is necessary to study the water injection volume that satisfies the corresponding requirements under different practical requirements. According to the different protection requirements for the shell plate and the first longitudinal bulkhead in reality, different weights are taken for the average deformation of the shell plate and the first longitudinal bulkhead, and the results are shown in Figure20.

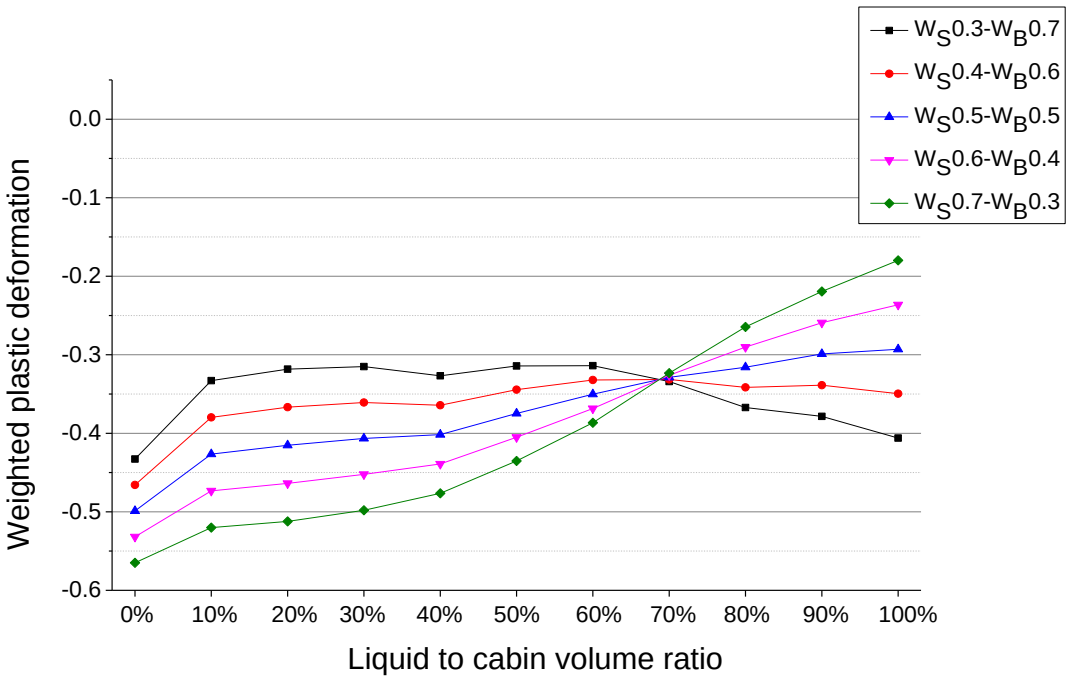

Figure 20. Weighted plastic deformation of the pontoon structure filled with water medium in protective tanks

In Figure 20, WS0.3-WB0.7 refers to the weighted plastic deformation value obtained by adding the average plastic deformation value of the shell plate (weighted 0.3) and the average plastic deformation value of the first longitudinal bulkhead (weighted 0.7), and the others are analogous. Five different weighting methods are used in Figure 20 to obtain different optimal results. It can be seen from the above figure that for any weighted method, when 70% of the water is injected into the protective tanks, the weighted plastic deformation of the structure is concentrated near -0.33, showing a special stability. In actual demand, if the user prefers to reduce the deformation of the shell plate over reducing the deformation of the first longitudinal bulkhead, the plastic deformation of the shell plate can be weighted by 0.7, so that the water injection volume that minimizes the weighted plastic deformation is 100%. Correspondingly, the plastic deformation value is reduced by 68.17% compared with the weighted plastic deformation value of the ordinary structure under the same weight condition. If the user prefers to reduce the deformation of the first longitudinal bulkhead over reducing the deformation of the shell plate, the plastic deformation of the first longitudinal bulkhead can be weighted by 0.7, so the water injection volume that minimizes the weighted plastic deformation is 60%. Correspondingly, the plastic deformation value is reduced by 27.46% compared with the weighted plastic deformation value of the ordinary structure under the same weight condition. If the damage to the shell plate and the first longitudinal bulkhead are equally important, then according to the result of weighing each of them at 0.5, the water injection volume that minimizes the weighted plastic deformation is 100%, and the plastic deformation value is 41.27% lower than that of an ordinary structure under the same weighted condition.

(2) Plastic deformation of pontoon structure with springs in protective tanks / Plastic deformation of spring-mounted pontoon structure in protective tanks

This section analyzes the plastic deformation of pontoon structures assembled with different types of springs in the protective tanks under the near-field explosion load. The dimensionless results of plastic deformation of the shell plate and first longitudinal bulkhead after assembling different types of springs in the protective tanks are shown in Figures 21 and 22.

The average values in Figures 21 and 22 refer to the average of the absolute values of the deformation at each observation point. According to the data for the average values in Figures 21 and 22, it can be seen that the maximum and minimum plastic deformations of the shell plate are the results of the protection of the Model 5 spring and the Model 4 spring, which are a reduction of 92.3% and 99.04%, respectively, compared with the data for the ordinary structure. The maximum and minimum plastic deformations of the first longitudinal bulkhead are the results of the protection of the Model 1 spring and the Model 3 spring, which are 82.95% and 92.43% lower than the data for the ordinary structure, respectively. There is no strong logical connection between the different models of the springs compared with the increasing volume of water in the protective tanks, so the curves in Figures 21 and 22 do not show a tendency for plastic deformation to vary with the spring type. Similar to the content in Model 1, the average deformation of the shell plate and the first longitudinal bulkhead are weighted differently, so the influence of the assembly spring in the protective tanks on the explosion-proof performance of the pontoon is comprehensively considered, as shown in Figure 23.

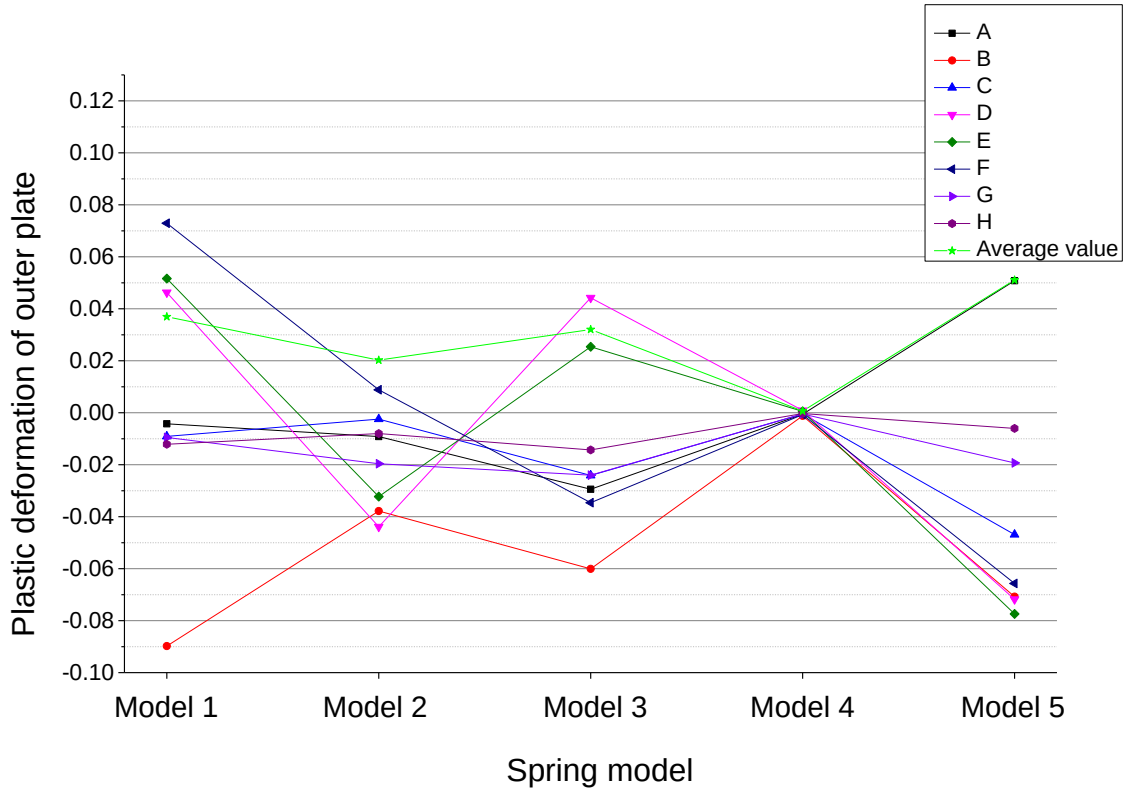

Figure 21. Plastic deformation of the shell plate of the pontoon with spring protection

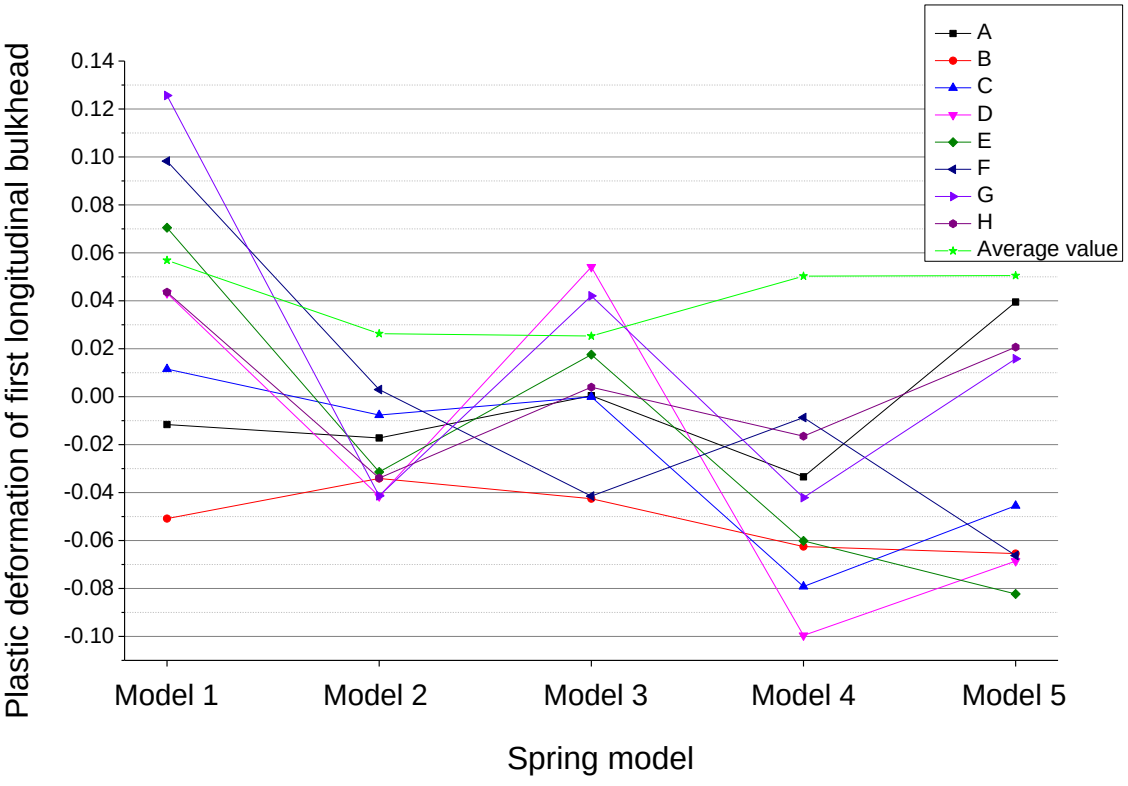

Figure 22. Plastic deformation of the first longitudinal bulkhead of the pontoon with spring protection

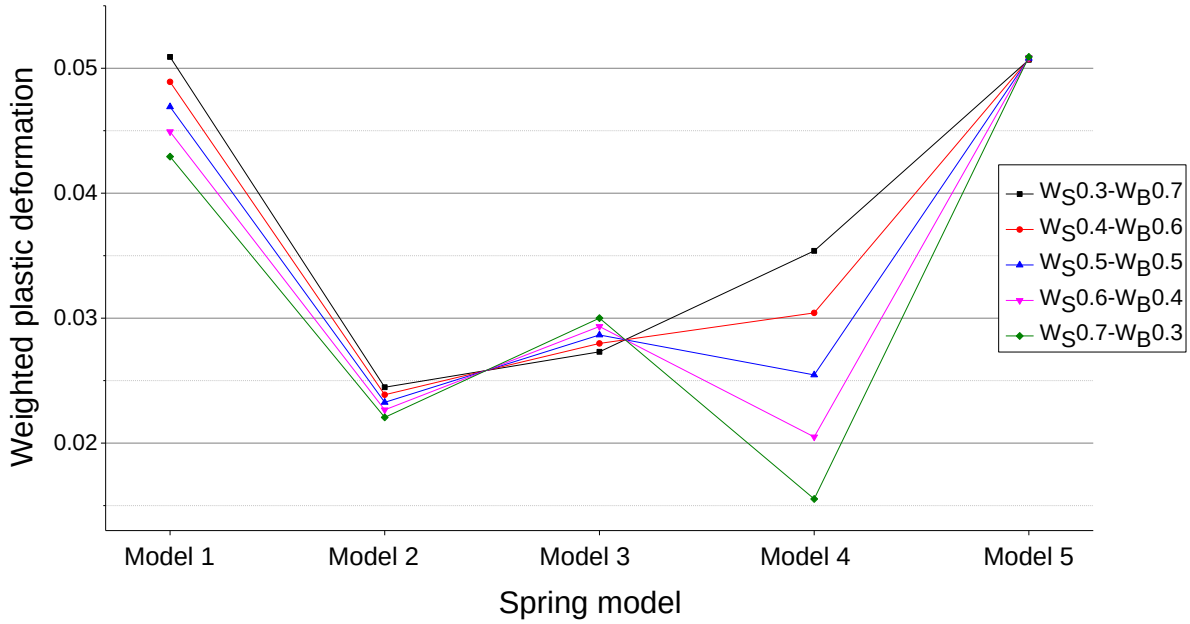

Figure 23. Weighted plastic deformation of the pontoon with spring protection

As can be seen in Figure 23, when the weighting method is WS0.3-WB0.7, WS 0.4-WB0.5, or WS0.5-WB0.5, the pontoon structure with the smallest weighted plastic deformation is the structure protected by the Model 2 spring. When the weighting method is WS0.6-WB0.4 or WS0.7-WB0.3, the pontoon structure with the smallest weighted plastic deformation is the structure protected by the Model 4 spring. It is worth mentioning that, according to the data in Figures 20 and 21, when the spring is assembled in the protective tanks, the deformation of both the shell plate and the first longitudinal bulkhead ranges from -0.1 to 0.13, which is an order of magnitude smaller than the data for the ordinary structure or the pontoons filled with the water medium. On the one hand, this indicates that the pontoon structure equipped with springs in the protective tanks is superior to the pontoon structure filled with the water medium in the protective tanks in terms of explosion-proof performance; on the other hand, it also indicates that all types of springs show excellent protection capabilities compared with the ordinary structure, and there is little difference in the protection effect between the different types of springs.

The pontoon structure equipped with springs in the protective tanks has such superior explosion-proof performance because, on the one hand, under the action of a detonation wave, the passive displacement of the shell plate causes the spring connected to it to undergo compression deformation, which consumes the energy transferred by the shell plate in the form of elastic potential energy. On the other hand, because of the dynamic displacement of the pontoon under the action of the detonation wave, the spring acts as a part of the pontoon and consumes a certain amount of kinetic energy when moving along with the pontoon, which is equivalent to increasing the inertial force of the pontoon and reducing its deformation and the response of velocity and acceleration. Furthermore, when the energy of the detonation wave is transmitted into the distance and its effect on the pontoon begins to decay, the elastic potential energy stored in the spring begins to be released, and the spring force acts on the shell plate and the first longitudinal bulkhead, so that its deformation can be restored to a large extent.

4.3 Energy of pontoon

To further compare the damage characteristics of each new pontoon structure under the action of a near-field explosion load, this section studies the energy of the pontoon structure. The energy data for the pontoon includes the kinetic and internal energy of the structure. To facilitate the comparison of results, the energy of the finite element model of the entire pontoon is extracted, that is, it includes the energy of all shell and beam elements of the structure but does not include the energy of the water or springs in the protective tanks. After the energy data is extracted, the normalization process is performed by the method of Equation 16, and the resulting data is as shown in Figures 24 and 25.

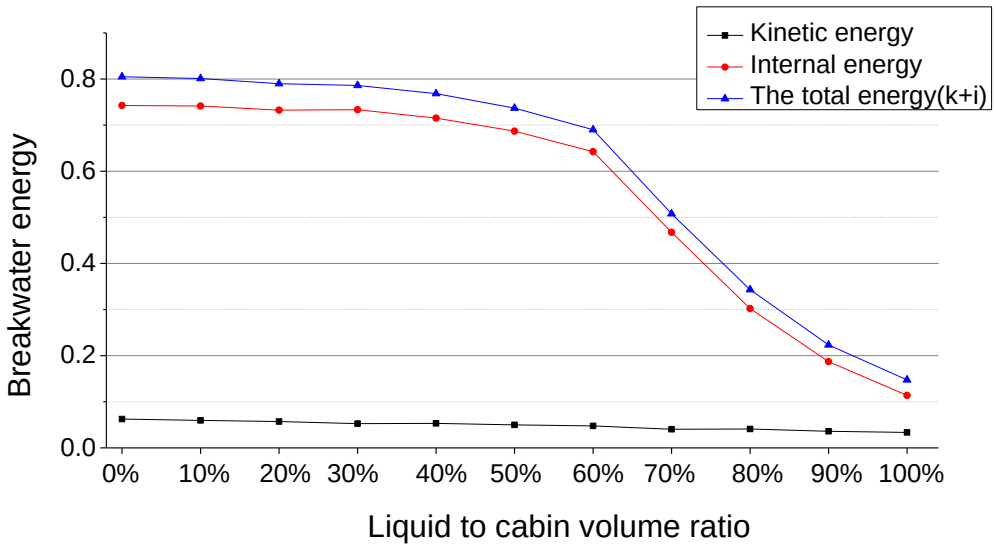

Figure 24. Energy of the pontoon structure filled with the water medium in the protective tanks

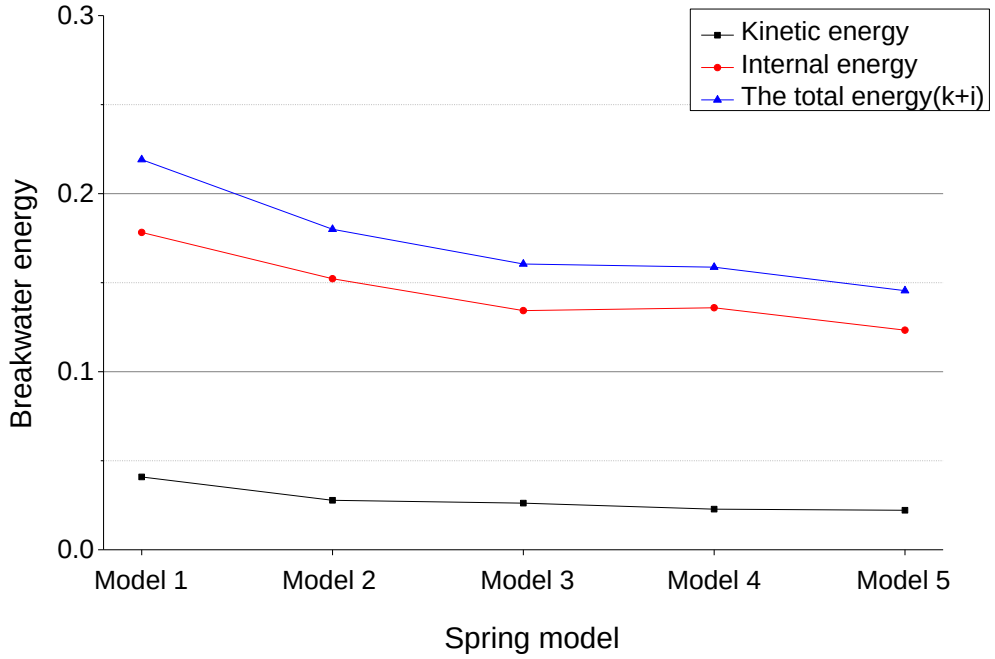

Figure 25. Energy of the pontoon structure with springs in the protective tanks

It can be seen from Figure 24 that the internal energy accounts for the largest proportion of the total energy of the explosion shock wave absorbed by the pontoon structure. For example, the internal energy accounted for 92.24% of the total energy of the ordinary pontoon structure. As the volume of water in the protective tanks increases, the kinetic and internal energy of the pontoon structure show a downward trend. The internal energy is especially likely to suffer a cliff-like drop after the water volume reaches 60% of the volume of the tanks. When the volume of water filling the protective tanks accounts for 90–100%, the total energy of the pontoon structure decreases to 18.31-27.7% of the energy of the ordinary structure. This means that the energy absorbed by the pontoon structure from the detonation wave is effectively reduced, and the damage caused by the detonation wave to the pontoon structure is also effectively reduced. The total energy of the pontoon structure equipped with five types of springs is controlled between 0.145J and 0.22J, which accounts for only 18.07-27.2% of the total energy of the ordinary structure. The protection effect is similar to that of the pontoon structure filled with 90-100% water in the protective tanks.

5. Conclusion

To enhance the role of pontoons in anti-terrorism efforts, this paper designs and calculates the damage characteristics of an ordinary pontoon structure and two new types of side-protection pontoon structures under a near-field explosion load. After analyzing the data of plastic deformation and energy of the structure, the following conclusions are drawn:

(1) The method of filling the protective tanks with the water medium has a protective effect on the pontoon, but the water volume corresponding to the minimum plastic deformation of the shell plate and the first longitudinal bulkhead under the near-field explosion load is not the same. According to the different requirements for the explosion-proof performance of the shell plate and the first longitudinal bulkhead in actual demand, the plastic deformation of the shell plate and the first longitudinal bulkhead can be weighted, and different water-filled volumes for the optimum explosion-proof performance of the pontoon can be obtained.

(2) The plastic deformation of the pontoon structure equipped with springs in the protective tanks is an order of magnitude smaller than that of the ordinary structure and the pontoon structure filled with the water medium in the protective tanks, which shows an excellent explosion-proof performance.

(3) As the volume of filled water in the protective tanks increases, the energy of the pontoon structure absorbing the detonation wave decreases.

(4) The energy of the pontoon structure equipped with springs in the protective tanks decreases to 18.07-27.2% of the energy of the ordinary structure, which is comparable to the protective effect of the pontoon structure filled with 90-100% of the water medium in the protective tanks.

REFERENCES

[1] Chen, C., Zhu, X., Hou, H., 2016. Research advance in damage load of fragmentized warhead exploded in air. *Ship Building of China*, 57(4), 197-214.

[2] Li, D., Hou, H., Chen, C., Zhu, X., Li, M., Yi, Q., 2018. Experimental study on the combined damage of multi-layered composite structures subjected to close-range explosion of simulated warheads. *International Journal of Impact Engineering*, 114, 133-146. https://doi.org/10.1016/j.ijimpeng.2017.12.007

[3] Wu, Z., Jin, H., Du, Z., Li, Y., 2019. Experimental studies of ship stiffened plates under the synergistic effects of fragments and shock wave. *Journal of Ship Mechanics*, 23(2), 211-217.

[4] Yin, Q., Li, S., Wang, K., 2017. Research on new ship bulkhead structure under impact damage load. *Ship Science and Technology*, 39(6), 6-11.

[5] Li, Y., Xiao, W., Cheng, Y., Li, J., Zhang, P., 2018. Numerical research on response of hybrid corrugated sandwich plates subjected to combined blast and fragment loadings. *Explosion and Shock Waves*, 38(2), 279-288.

[6] Zhao, L., Chen, J., Liu, S., 2013. Residual Characteristics of the Fragments Penetrating Protective Side Tanks. *Chinese Journal of Ship Research*, 8(06), 40-44.

[7] Kong, X., Wu, W., Liu, F., Tan, H., Tao, J., 2014. Research on protective effect of guarding fluid tank under attacking by explosion fragments. *Journal of Ship Mechanics*, 18(08), 996-1004.

[8] Wang, Y., Liu, Y., Zhang, A., Tian, Z., 2013. Research on protective performance of different shipboard structures subjected to air contact explosion with ANSYS/LS-DYNA. *Ship Science and Technology*, 35(07), 25-31.

[9] Yuan, P., Zhao, Y., 2017. Numerical simulation of damage to ship structure by underwater contact explosion shock wave. *Chemical Engineering Transactions*, 62, 673-678.

[10] Yongkun, Z., Xin, G., 2017. Research on the ship local structure damage subjected to underwater explosion. *29th Chinese Control And Decision Conference (CCDC)*, Chongqing, China. https://doi.org/10.1109/CCDC.2017.7978269

[11] Guan, Y., Fang, S., Zhao, S., Shi, T., Dong, Y., 2018. Study on Dynamic Response of Cargo Hold Structure of CNG Carriers under Gas Explosion Loading. *Journal of Ship Mechanics*, 22(3), 374-385.

[12] Zhang, Y., Chen, F., Han, Y., 2018. Simulation Study on the Deflection Response of the 921A Steel thin plate under Explosive Impact Load. *International Symposium on Application of Materials Science and Energy Materials (SAMSE)*, Shanghai, China. https://doi.org/10.1088/1757-899X/322/2/022054

[13] Chen, P., Wei, Q., Liu, Z., 2018. The Influence Analysis of Flat Steel on Explosive Loading inside Closed Cabin. *28th International Ocean and Polar Engineering Conference*, Sapporo, Japan.

[14] Liu, Y. L., Zhang, A. M., Tian, Z. L., Wang, S. P., 2018. Numerical investigation on global responses of surface ship subjected to underwater explosion in waves. *Ocean Engineering*, 161, 277-290. https://doi.org/10.1016/j.oceaneng.2018.05.013

[15] Ming, F. R., Zhang, A. M., Xue, Y. Z., Wang, F. S., 2016. Damage characteristics of ship structures subjected to shockwaves of underwater contact explosions. *Ocean Engineering*, 117, 359-382. https://doi.org/10.1016/j.oceaneng.2016.03.040

[16] Veić, D., Wojciech S., Rohan S., 2019. Effect of Breaking Wave Shape on Impact Load on a Monopile Structure. *Brodogradnja*, 70(2), 25-42. https://doi.org/10.21278/brod70302

[17] Jiang, G., Jin, H., Wang, Y., Zhou, X., 2010. Study on shock response of floating platform subjected to far-field explosion. *Acta Armamentarii*, 31(SUPPL. 1), 37-40.

[18] Yang, Z., Xie, M., Gao, Z., Xu, T., Guo, W., Ji, X., Yuan, C., 2018. Experimental investigation on hydrodynamic effectiveness of a water ballast type pontoon. *Ocean Engineering*, 167, 77-94. https://doi.org/10.1016/j.oceaneng.2018.08.030

[19] He, F., Zhang, H., Zhao, J., Zheng, S., Iglesias, G., 2019. Hydrodynamic performance of a pile-supported OWC breakwater: An analytical study. *Ocean Engineering*, 88, 618-626. https://doi.org/10.1016/j.oceaneng.2014.04.023

[20] Yang, Z., Xie, M., Hou, Z., Ji, X., Guo, W., He, F., 2017. An Experimental Study of the Hydrodynamic Performance on the Anti-rolling Type Floating Breakwater, 27th International Ocean and Polar Engineering Conference, San Francisco, USA.

[21] Duan, W., Xu, S., Xu, Q., Ertekin, R. C., Ma, S., 2017. Performance of an F-type pontoon: A numerical and experimental study. *Proceedings of the Institution of Mechanical Engineers Part M: Journal of Engineering for the Maritime Environment*, 231(2), 583-599. https://doi.org/10.1177/1475090216673461

[22] Deng, Z., Wang, L., Zhao, X., Huang, Z., 2019. Hydrodynamic performance of a T-shaped pontoon. *Applied Ocean Research*, 82, 325-336. https://doi.org/10.1016/j.apor.2018.11.002

[23] Dai, J., Wang, C. M., Utsunomiya, T., Duan, W., 2018. Review of recent research and developments on pontoons. *Ocean Engineering*, 158, 132-151. https://doi.org/10.1016/j.oceaneng.2018.03.083

[24] Chen, F., Wang, C., Zhou, D., 2012. Review of theory and numerical methods of fluid-structure interaction. *Spatial Structures*,18(04), 55-63.

[25] Wang H., Cheng Y. S., Pei D. M., Hao W. W., Gan L., 2019. Water Entry Hydroelasticity Analysis of Lattice Sandwich Panel with Imperfection:Simulation and Engineering Model. *Brodogradnja*, 70(2), 25-42. https://doi.org/10.21278/brod70203

[26] Naumyenko, I., Petroskyi, I., 1956. The shock wave of a nuclear explosion. BOEH, CCCP.

Submitted: 12.02.2022.
Accepted: 12.10.2022.

Kai Li, likai@dlut.edu.cn
School of Naval Architecture and Ocean Engineering, Dalian University of Technology, Dalian 116024, China
Zhichao Zhao
School of Naval Architecture and Ocean Engineering, Dalian University of Technology, Dalian 116024, China
Songliang Chang
School of Naval Architecture and Ocean Engineering, Dalian University of Technology, Dalian 116024, China
Jiawei Bao
School of Naval Architecture and Ocean Engineering, Dalian University of Technology, Dalian 116024, China
Zhijiang Yuan
Department of Navigation, Dalian Naval Academy, Dalian 116001, China
Xiaogang Jiang
Department of Navigation, Dalian Naval Academy, Dalian 116001, China